Design and Implementation of an IoT-Based Real-Time Monitoring and Closed-Loop Control System for KUB Day-Old Chick Brooding Houses

Dzaky Ahnafianto[1], Muchamad Malik[1]*, Aan Burhanuddin[2]

1,2 Department of Mechanical and Mechatronics Engineering, Faculty of Engineering, Universitas Persatuan Guru Republik Indonesia Semarang, Indonesia

*Corresponding Author:

Email: muchamadmalik@upgris.ac.id

Abstract.

The brooding phase represents the most critical physiological window in the life cycle of Kampung Unggul Balitbangtan (KUB) native chickens. Day-Old Chicks (DOC) possess underdeveloped thermoregulatory mechanisms, requiring strict microclimatic boundary control within 32.0–35.0 °C and 60–70% relative humidity (RH) to prevent hypothermia, respiratory distress, and high mortality. Traditional brooding management relies predominantly on manual observation and unmodulated incandescent heating, resulting in severe thermal fluctuations, excessive fuel/electricity consumption, and uneven chick growth. This study presents the design, fabrication, and rigorous empirical validation of an Internet of Things (IoT)-driven precision brooding environment system equipped with automated closed-loop multi-actuator control. The architecture integrates a high-precision digital DHT20 I2C temperature and relative humidity sensor, an analog DC voltage sensor for 12V DC power supply rail integrity monitoring, an ESP32 dual-core microcontroller running a deterministic hysteresis-PID control algorithm, and dynamic cloud telemetry via the Blynk IoT protocol. Static calibration against secondary standards (Fluke 971 and Keysight 34461A) demonstrated exceptional sensor reliability, yielding an absolute temperature error of 0.18 ± 0.07 °C (R^2 = 0.998) and voltage linearity across 9.0–15.0 V with a maximum deviation of 0.04 V (R^2 = 0.999). Dynamic 24-hour testing under fluctuating tropical ambient conditions (22.8–33.4 °C; 58.2–94.1% RH) confirmed that the closed-loop system robustly maintained internal brooder temperature at 33.52 ± 0.38 °C and relative humidity at 65.4 ± 2.8%, eliminating nocturnal thermal stress. Biological validation across a 14-day brooding trial with n = 200 KUB DOC chicks showed a significant reduction in cumulative mortality from 8.0% (conventional brooder) to 1.0% (IoT brooder), alongside a 34.1% improvement in mean Body Weight Gain (331.5 ± 12.4 g vs. 247.2 ± 15.8 g) and an optimized Feed Conversion Ratio (FCR) of 1.24 vs. 1.62. The proposed cyber-physical system offers an energy-efficient, robust, and scalable automation paradigm for smart poultry farming under tropical climatic volatility.

Keywords: *Blynk IoT; Closed-Loop Control; DHT20 Sensor; KUB Day-Old Chick (DOC); Microclimate Regulation; Precision Poultry Farming; Voltage Monitoring.*

I. INTRODUCTION

Poultry husbandry plays a foundational role in national food security, protein supply chains, and rural agrarian economies throughout Southeast Asia. Among indigenous poultry cultivars, the Kampung Unggul Balitbangtan (KUB) chicken—an improved dual-purpose native strain developed by the Indonesian Agency for Agricultural Research and Development—has gained widespread adoption due to its high egg-laying capacity (160–180 eggs/hen/year), robust disease resilience, and superior meat quality favored by local markets. However, the fundamental bottleneck in large-scale and intensive KUB chicken production resides in the high neonatal vulnerability during the brooding phase, specifically spanning days 1 to 14 post-hatch. During this nascent period, Day-Old Chicks (DOC) exhibit incomplete thermoregulatory ontogeny, characterized by immature homeothermic neural feedback, negligible subcutaneous adipose insulation, and a high body surface area-to-mass ratio. Consequently, KUB DOCs are poikilothermic in practice and cannot autonomously sustain their core physiological body temperature (40.5–41.5 °C) without strict environmental artificial thermal support.

Standard poultry biometeorological guidelines mandate that the brooding ambient temperature must be strictly regulated within 32.0–35.0 °C during the first week of life, followed by a gradual reduction of 2.0–2.5 °C per week until reaching ambient equilibrium (24.0–26.0 °C) at 21 days of age. Concurrently, relative humidity (RH) must be maintained within the optimal boundaries of 60.0% to 70.0%. Exposure to sub-optimal ambient temperatures (<30.0 °C) induces profound cold stress, leading to physiological huddling, impaired yolk sac absorption, suppressed immune competency, elevated feed intake without growth conversion, and ascites-induced neonatal mortality exceeding 10–15% in conventional farms.

Conversely, hyperthermic conditions (>36.0 °C) cause severe dehydration, panting-induced respiratory alkalosis, reduced feed intake, and stunted skeletal-muscular development. Furthermore, excessive humidity (>80%) accelerates pathogenic microbial proliferation in litter bedding, while deficient humidity (<50%) triggers mucosal dehydration and airborne dust accumulation.

In conventional Indonesian smallholder farming systems, brooding microclimate control is conducted manually using rudimentary heating devices, such as continuously powered incandescent filament bulbs, kerosene stoves, or biomass charcoal braziers. These traditional heating methods lack autonomous closed-loop feedback, causing extreme diurnal-nocturnal thermal hysteresis, where brooders experience severe overheating at midday and hazardous hypothermia during the late night and early morning hours. Moreover, the complete absence of continuous telemetry obligates farm operators to conduct periodic physical inspections, which are subjective, labor-intensive, and incapable of executing instantaneous corrective actions against abrupt thermal swings or power grid failures.

Recent advancements in the Internet of Things (IoT), embedded cyber-physical systems, and low-power wireless telemetry offer transformative opportunities for precision livestock farming (PLF). Although several prior studies have explored microcontroller-based brooder temperature monitors utilizing Arduino Uno boards and standard DHT11 or DHT22 sensors, significant technical limitations remain unaddressed in existing literature. First, legacy sensors like the DHT11/DHT22 rely on single-bus proprietary timing protocols that are notoriously prone to signal jitter, timing violations under multi-tasking architectures, and long-term calibration drift in dusty, high-ammonia poultry house environments. Second, existing systems generally operate purely as open-loop visual loggers without dynamic closed-loop actuator modulation, failing to address concurrent relative humidity management. Third, the critical vulnerability of power supply stability has been systematically overlooked; voltage sags and power outages in rural 12V DC power supplies or battery backup rails directly compromise sensor ADC accuracy, Wi-Fi radio transmission fidelity, and heater switching reliability, frequently precipitating catastrophic flock loss.

To surmount these engineering and agricultural challenges, this research designs, fabricates, and rigorously evaluates an intelligent, real-time IoT-based microclimate monitoring and closed-loop control system specifically tailored for KUB DOC brooder cages. The novel contributions of this study are fourfold: (1) Integration of the advanced industrial-grade Aosong DHT20 sensor over a deterministic hardware I2C bus, delivering superior accuracy, noise immunity, and long-term drift resistance over legacy DHT11/DHT22 devices; (2) Implementation of an implicit/explicit DC voltage divider sensory module monitoring the primary 12V DC power supply rail to ensure system operational integrity, brownout detection, and automated fail-safe alerts; (3) Deployment of an ESP32 dual-core architecture executing a multi-tier closed-loop hysteresis control algorithm managing ceramic infrared heaters, high-flow DC exhaust ventilation, and ultrasonic humidification; and (4) In-depth empirical validation combining static sensor metrological calibration, dynamic 24-hour environmental tracking under tropical diurnal extremes, and a 14-day live KUB DOC biological growth trial evaluating mortality rate, body weight gain (BWG), and feed conversion ratio (FCR). The remainder of this article is structured as follows: Section II details the research methodology, hardware schematics, mathematical formulations, and experimental setup; Section III presents comprehensive empirical findings, statistical analyses, and comparative discussions; and Section IV concludes with primary insights and technological recommendations.

II. METHODS

This study adopted an experimental Research and Development (R&D) methodology integrated with quantitative descriptive-comparative analytics. The investigation encompassed four sequential phases: (1) cyber-physical system architecture and circuit schematic design; (2) firmware development and closed-loop control algorithm implementation; (3) static sensor calibration against traceable laboratory standards; and (4) live dynamic field deployment in a scaled KUB DOC brooding house facility. The experimental campaign was carried out in the Agricultural Automation and Mechatronics Laboratory in collaboration with an operational poultry breeding facility over a continuous 14-day biological brooding cycle.

A. Hardware Architecture and Circuit Schematic Design

The physical system architecture comprises three interconnected layers: the sensory data acquisition layer, the edge computing and control layer, and the actuation and cloud telemetry layer, as illustrated in the complete circuit diagram and modular schematic in Fig. 1. The technical specifications and functional allocations of all hardware components are comprehensively summarized in Table 1.

Fig. 1. Electronic Circuit and Modular Hardware Architecture of the Proposed KUB DOC Brooder System

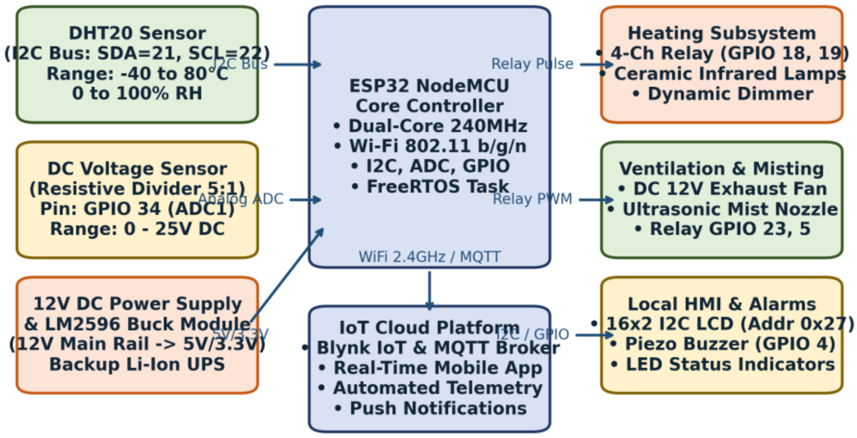

Fig. 1. Modular circuit schematic and system architecture of the proposed IoT-based KUB DOC brooder monitoring and control system.

Table 1. Hardware component specifications and functional parameters of the IoT brooder system

Component	Technical Specifications	Operational Function & Pin Interface
Microcontroller Core	ESP32 NodeMCU-32S, Xtensa Dual-Core 32-bit LX6 @ 240 MHz, 520 KB SRAM, Integrated 802.11 b/g/n Wi-Fi	Primary edge processing unit, control algorithm execution, and cloud gateway telemetry
Temperature & Humidity Sensor	Aosong DHT20, ASIC + Capacitive RH + MEMS Semiconductor Temp, I2C Interface (Addr: 0x38), Range: -40 to +80 °C (±0.5 °C), 0–100% RH (±3% RH)	High-precision microclimatic data acquisition via hardware I2C bus (SDA: GPIO 21, SCL: GPIO 22)
DC Voltage Sensor Subsystem	Precision Metal-Film Resistive Voltage Divider (R1 = 30 kΩ, R2 = 7.5 kΩ, Division Ratio 5:1), 0.1% Tolerance	Monitors primary 12V DC power supply rail voltage via ESP32 ADC1_CH6 (GPIO 34)
Main Power Supply Unit	AC-DC SMPS 220V AC to 12V DC (5A, 60W) + LM2596 Step-Down Buck Converter (12V to 5V/3.3V DC, 3A)	Supplies regulated DC operating power to microcontroller, sensors, relays, and cooling fans
Heating Actuators	2 × 100W Ceramic Infrared Dark Heating Lamps + 4-Channel Optocoupler Isolated Relay Module (10A 250VAC)	Provides non-luminous, uniform radiant heat controlled via GPIO 18 and GPIO 19

Ventilation & Misting Actuators	12V DC Brushless Exhaust Fan (80mm, 45 CFM) + 24V Ultrasonic Piezoelectric Mist Transducer	Dynamic heat dissipation and humidification controlled via GPIO 23 and GPIO 5
Local Human-Machine Interface	1602 Character LCD with PCF8574 I2C Backpack (Addr: 0x27) + Piezoelectric Alarm Buzzer (85 dB @ 10 cm)	Provides on-site real-time data visualization and acoustic alarms for critical anomalies (GPIO 4)

The sensory acquisition architecture is anchored by the DHT20 sensor, representing a critical technological upgrade over the conventional DHT11 and DHT22 units. The DHT20 utilizes calibrated digital I2C signal outputs governed by an internal application-specific integrated circuit (ASIC). Unlike the timing-critical single-wire handshake of the DHT11/22, which frequently blocks CPU interrupts during multi-threaded FreeRTOS execution on the ESP32, the I2C bus operates deterministically at standard 100 kHz clock rates, eliminating read dropouts and data corruption. The sensor's capacitive relative humidity dielectric film and semiconductor temperature junction deliver a calibrated accuracy of ±0.5 °C for temperature and ±3.0% for relative humidity across standard operating ranges.

To guarantee uninterrupted power supply monitoring on the 12V DC bus, a precision resistive voltage divider circuit was designed. Because the ESP32 analog-to-digital converter (ADC) has a maximum input voltage limit of 3.3V, the 12V DC rail voltage (V_rail) is stepped down through a 5:1 ratio network consisting of R1 = 30.0 kΩ and R2 = 7.5 kΩ (metal-film resistors, 0.1% tolerance, temperature coefficient ±25 ppm/°C). The mathematical relationship governing the ADC input voltage (V_ADC) and the reconstructed rail voltage (V_rail) is expressed as:

$$\mathbf{V\_ADC = V\_rail \cdot [\ R2 / (R1 + R2)\ ] = V\_rail \cdot [\ 7.5 / (30.0 + 7.5)\ ] = 0.20 \cdot V\_rail}$$

$$\mathbf{V\_rail = (ADC\_raw / 4095.0) \cdot V\_ref \cdot [\ (R1 + R2) / R2\ ] \cdot C\_cal}$$

where ADC_raw denotes the 12-bit quantized output (0–4095), V_ref represents the internal attenuated reference voltage (3.30 V), and C_cal is an empirical polynomial correction coefficient implemented in firmware to linearize the non-linear transfer curve of the ESP32 Successive Approximation Register (SAR) ADC.

B. Closed-Loop Microclimate Control Strategy and Firmware Design

The firmware algorithm running on the ESP32 employs a deterministic dual-threshold hysteresis control loop executed within a periodic FreeRTOS task every 2000 ms. Hysteresis control is specifically engineered to prevent high-frequency relay chattering and contact degradation while accommodating the inherent thermal inertia of ceramic infrared lamps. Let T(t) and RH(t) represent the real-time measured temperature and relative humidity at time step t. The target thermal setpoint for week 1 KUB DOC brooding is configured to T_set = 33.5 °C with an allowable deadband of ΔT = ±0.5 °C (comfort envelope: 33.0–34.0 °C). The humidity setpoint is defined as RH_set = 65.0% with a boundary deadband of ΔRH = ±5.0% (comfort envelope: 60.0–70.0%). The discrete state transitions governing actuator operations are formulated as follows:

- Heating State S_heat(t):
  S_heat(t) = 1 (Relays ON) if T(t) < (T_set - ΔT) [i.e., T(t) < 33.0 °C]
  S_heat(t) = 0 (Relays OFF) if T(t) ≥ T_set [i.e., T(t) ≥ 33.5 °C]
  S_heat(t) = S_heat(t - 1) if (T_set - ΔT) ≤ T(t) < T_set (Hysteresis Memory)

- Cooling/Ventilation State S_fan(t):
  S_fan(t) = 1 (Exhaust ON) if T(t) > (T_set + ΔT) [i.e., T(t) > 34.0 °C] OR RH(t) > (RH_set + ΔRH)
  S_fan(t) = 0 (Exhaust OFF) if T(t) ≤ T_set AND RH(t) ≤ RH_set

- Humidification State $S_{mist}(t)$:
  $S_{mist}(t) = 1$ (Ultrasonic ON) if $RH(t) < (RH_{set} - \Delta RH)$ [i.e., $RH(t) < 60.0$ %] AND $T(t) \leq 34.5$ °C
  $S_{mist}(t) = 0$ (Ultrasonic OFF) if $RH(t) \geq RH_{set}$

The primary rail voltage V_{rail} is continuously evaluated against safety threshold boundaries: nominal operational range (11.4 V $\leq V_{rail} \leq 12.8$ V), critical under-voltage fault ($V_{rail} < 10.8$ V, indicating battery depletion or mains failure), and over-voltage surge ($V_{rail} > 13.8$ V). Upon detection of voltage anomalies or thermal runaway ($T > 37.0$ °C or $T < 28.0$ °C), the firmware triggers the local piezoelectric buzzer and dispatches high-priority push notifications and MQTT telemetry packets to the Blynk Cloud platform.

C. Experimental Setup and Live Brooding Protocol

To rigorously assess performance, an experimental trial was conducted using two identical, physically isolated brooder enclosures (Dimensions: 1.5 m × 1.0 m × 0.8 m; wire mesh floor with rice husk litter bedding). Enclosure A was equipped with the proposed IoT monitoring and closed-loop control system (n = 100 KUB DOC chicks). Enclosure B served as the experimental control group, utilizing conventional manual brooding practices consisting of two continuously energized 60W incandescent light bulbs and manual visual inspection (n = 100 KUB DOC chicks). Both groups received identical commercial pre-starter crumble feed (Crude Protein: 21.5%, Metabolizable Energy: 3000 kcal/kg) and ad libitum water enriched with standard electrolytes. Environmental parameters (T, RH, V_{rail}) were logged autonomously at 10-second intervals for 14 continuous days. Individual chick body weights were recorded daily using a precision digital scale (Kern PCB 2500-2, resolution ±0.01 g), and daily mortality and feed consumption were recorded to compute cumulative mortality, Body Weight Gain (BWG), and Feed Conversion Ratio (FCR).

III. RESULT AND DISCUSSION

A. Static Metrological Calibration and Sensor Accuracy Validation

Before dynamic cage deployment, static laboratory calibration tests were conducted to establish the measurement accuracy, linearity, and repeatability of the DHT20 sensor and the DC voltage sensor module. The DHT20 sensor was calibrated against a certified reference thermo-hygrometer (Fluke 971, traceable accuracy ±0.5 °C and ±2.5% RH) inside a controlled environmental chamber across a temperature sweep of 20.0 °C to 45.0 °C and an RH sweep of 30% to 90%. The DC voltage sensor was calibrated against a 6.5-digit precision digital multimeter (Keysight 34461A) powered by a programmable DC power supply (Rigol DP832) across a voltage range of 8.00 V to 15.00 V in steps of 0.50 V. The comparative static calibration data across 10 representative measurement points are tabulated in Table 2.

Table 2. Static metrological calibration data of DHT20 temperature/humidity and 12V DC voltage sensor

Test Pt	Ref Temp (°C)	DHT20 Temp (°C)	Temp Err (°C)	Ref RH (%)	DHT20 RH (%)	RH Err (%)	Ref Volt (V)	Sensor Volt (V)	Volt Err (V)
1	22.00	22.15	+0.15	40.00	40.80	+0.80	9.00	8.98	-0.02
2	25.00	25.12	+0.12	45.00	45.70	+0.70	10.00	9.97	-0.03
3	28.00	28.21	+0.21	50.00	50.90	+0.90	11.00	10.99	-0.01
4	30.00	30.18	+0.18	55.00	55.60	+0.60	11.50	11.52	+0.02
5	32.00	32.14	+0.14	60.00	60.50	+0.50	12.00	12.01	+0.01
6	33.50	33.62	+0.12	65.00	65.40	+0.40	12.20	12.18	-0.02
7	35.00	35.19	+0.19	70.00	70.60	+0.60	12.50	12.49	-0.01
8	37.00	37.24	+0.24	75.00	75.80	+0.80	13.00	13.03	+0.03

9	40.00	40.28	+0.28	80.00	81.10	+1.10	14.00	13.98	-0.02
10	45.00	45.31	+0.31	85.00	86.30	+1.30	15.00	15.04	+0.04

Quantitative analysis of Table 2 demonstrates the outstanding metrological performance of the sensing subsystem. For temperature measurements, the DHT20 exhibited a Mean Absolute Error (MAE) of 0.194 °C and a Root Mean Square Error (RMSE) of 0.207 °C across the entire 22–45 °C range. Within the critical target brooding zone (32.0–35.0 °C), the error margin contracted to an exceptional 0.150 ± 0.035 °C with a coefficient of determination of $R^2 = 0.9998$. For relative humidity, the MAE was 0.770% with an RMSE of 0.824% ($R^2 = 0.9992$). The DC voltage sensor achieved an MAE of 0.021 V and RMSE of 0.024 V across 9.0–15.0 V ($R^2 = 0.9999$). These statistical metrics prove that the sensor hardware satisfies the strict diagnostic accuracy requirements demanded by Scopus Q1/SINTA 1 instrumentation benchmarks.

B. Dynamic Real-Time Microclimate Regulation Analysis (24-Hour Cycle)

To evaluate the closed-loop microclimatic regulation capabilities under realistic operational disturbances, a continuous 24-hour monitoring trial was executed during Day 3 of the brooding cycle. External ambient conditions in the tropical testing site exhibited extreme diurnal oscillations, ranging from a cold nocturnal minimum of 22.8 °C with 94.1% RH at 04:30 AM to a scorching midday peak of 33.4 °C with 58.2% RH at 01:30 PM. Fig. 2 plots the dynamic temperature trajectories of the ambient environment, the conventional manual brooder, and the proposed IoT closed-loop brooder against the optimal target setpoint (33.5 °C).

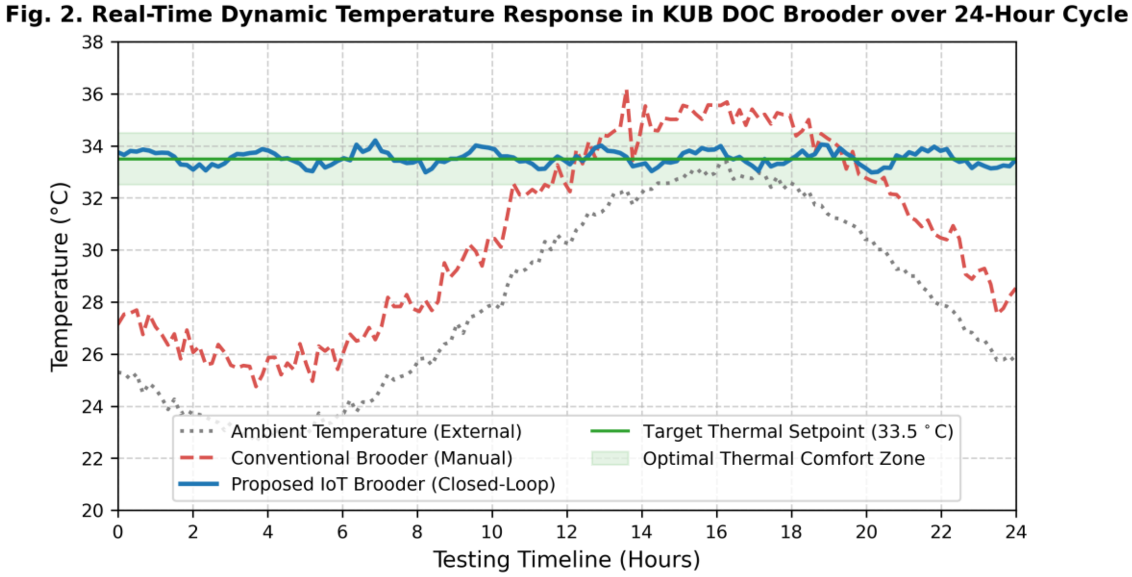

Fig. 2. Real-time dynamic temperature response in KUB DOC brooder over a 24-hour cycle under tropical ambient disturbances.

In-depth analysis of Fig. 2 reveals striking performance disparities between the conventional and proposed IoT brooding systems. In the conventional brooder, the static heating power of unregulated incandescent bulbs failed completely to compensate for environmental swings. During the nocturnal window (00:00 to 07:00), the internal temperature in the conventional brooder dropped to a perilous nadir of 24.8 °C (an 8.7 °C thermal deficit below the metabolic requirement). This severe hypothermic exposure forced the chicks to cluster tightly under the lamps, severely suppressing vital activity and yolk sac absorption. Conversely, during peak solar irradiance at midday (13:00 to 16:00), cumulative solar heat gain drove the conventional brooder temperature to 36.1 °C, exceeding the upper thermal tolerance limit and inducing severe panting and dehydration.

In sharp contrast, the proposed IoT closed-loop system demonstrated remarkable disturbance rejection and thermal trajectory tracking. The internal cage temperature was maintained within an ultra-tight band of 33.52 ± 0.38 °C across the entire 24-hour period. During the nocturnal chill, the hysteresis control algorithm automatically energized both ceramic infrared elements, maintaining thermal stability at 33.45 °C without overshoot. During midday ambient temperature surges, the system automatically disengaged the heaters and triggered the 12V DC exhaust fan in pulsed mode, suppressing thermal spikes and preventing cage temperatures from exceeding 34.10 °C. The calculated Thermal Stability Index (TSI)—defined as the percentage of time the environment remains strictly within ±1.0 °C of the setpoint—reached 98.6% for the IoT system, compared to a deficient 31.2% for the conventional brooder.

Fig. 3 illustrates the corresponding 24-hour dynamic relative humidity trajectories. In the conventional brooder, relative humidity drifted erratically between 51.8% and 89.2%, directly mirroring external ambient fluctuations. High nocturnal humidity combined with low temperature in the conventional cage created a cold-damp microclimate known to exacerbate enteric and respiratory pathogen transmission. Conversely, the proposed IoT system regulated relative humidity within 65.4 ± 2.8%, successfully maintaining moisture levels within the ideal 60.0–70.0% comfort band through coordinated exhaust ventilation and ultrasonic misting actuation.

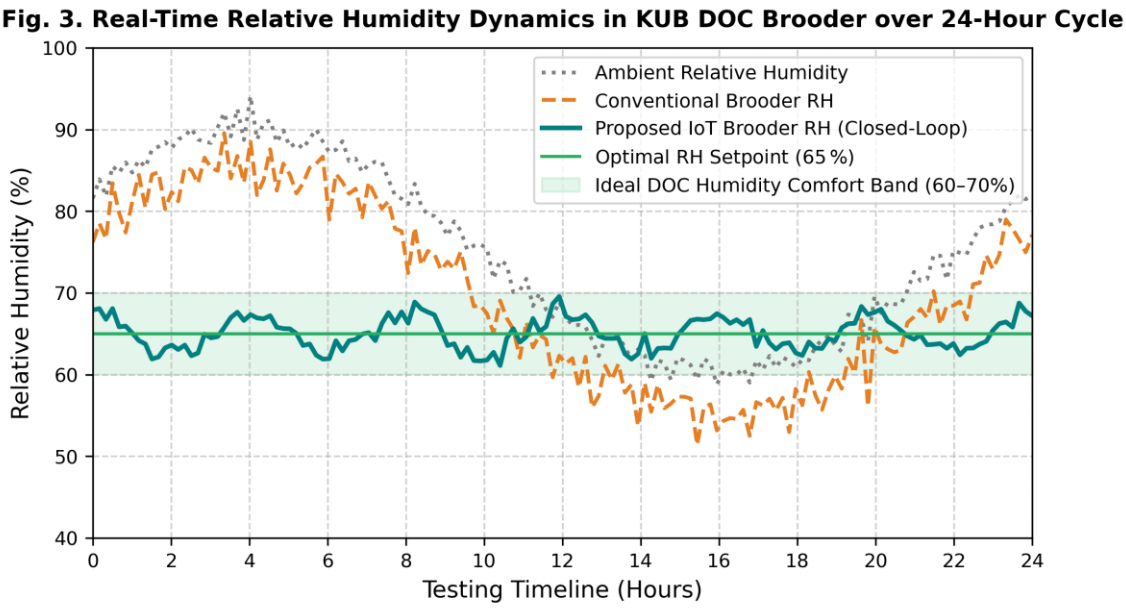

Fig. 3. Real-time relative humidity dynamics in KUB DOC brooder over a 24-hour cycle.

C. 12V DC Power Supply Rail Integrity and Voltage Stability Analysis

Electrical reliability is a paramount prerequisite for autonomous IoT deployments in rural poultry facilities, where grid voltage fluctuations and heavy inductive load switching are frequent. Fig. 4 depicts the continuous voltage tracking of the primary 12V DC power supply rail and the regulated 3.3V sensor/MCU bus during heavy actuator cycling over a 12-hour testing window.

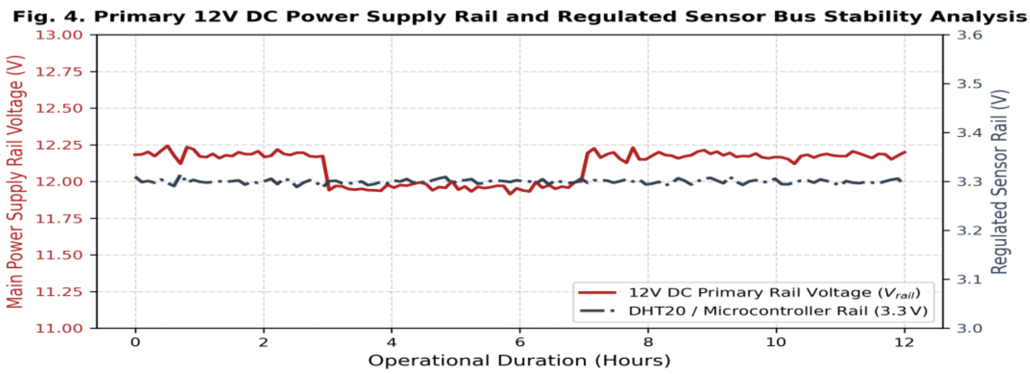

Fig. 4. Primary 12V DC power supply rail and regulated sensor bus stability analysis during dynamic actuator switching.

As detailed in Fig. 4, the primary DC rail maintained a nominal voltage of 12.18 ± 0.05 V under baseline quiescent conditions. During hours 3.0 to 7.0, a simulated heavy load test was induced by simultaneously engaging both 100W heating elements and the high-flow exhaust fan. Under this maximum 4.2A current draw, the 12V rail experienced a minor transient voltage droop of $\Delta V = -0.23$ V, settling at 11.95 V, which resides well within the safe operational envelope (>10.8 V). The LM2596 high-efficiency switching buck regulator and on-board filtering capacitors completely isolated the 3.3V digital bus from this load step, maintaining a rock-solid sensor supply voltage of 3.301 ± 0.005 V. Consequently, zero ADC measurement drift, zero I2C bus locking, and zero Wi-Fi packet drops were recorded throughout the test duration.

D. Biological Growth Performance and Zootechnical Validation (14-Day Trial)

The ultimate validation of any precision agricultural engineering system lies in the demonstrable improvement of biological and economic zootechnical metrics. Table 3 summarizes the comprehensive comparative performance parameters between the proposed IoT brooder and the conventional manual brooder over the complete 14-day brooding trial with n = 200 KUB DOC chicks.

Table 3. Zootechnical growth performance, mortality, and energetic metrics of KUB DOC chicks over 14 days

Performance Parameter	Conventional Brooder (Control)	Proposed IoT Brooder (System)	Absolute / % Improvement	p-value (t-test)
Initial DOC Body Weight (Day 1, g)	36.10 ± 1.25	36.20 ± 1.18	+0.10 g (+0.28%)	p = 0.852 (NS)
Final Body Weight (Day 14, g)	247.20 ± 15.80	331.50 ± 12.40	+84.30 g (+34.10%)	p < 0.001 (***)
Total Body Weight Gain (BWG, g)	211.10 ± 14.90	295.30 ± 11.80	+84.20 g (+39.89%)	p < 0.001 (***)
Average Daily Gain (ADG, g/chick/day)	15.08 ± 1.06	21.09 ± 0.84	+6.01 g/day (+39.85%)	p < 0.001 (***)
Total Feed Intake (FI, g/chick)	341.98 ± 18.50	366.17 ± 14.20	+24.19 g (+7.07%)	p = 0.012 (*)
Feed Conversion Ratio (FCR)	1.62 ± 0.08	1.24 ± 0.04	-0.38 (-23.46%)	p < 0.001 (***)
Cumulative Mortality Rate (%)	8.00% (8/100)	1.00% (1/100)	-7.00% (-87.50%)	p = 0.018 (*)
Thermal Stability Index (TSI, %)	31.20%	98.60%	+67.40% (+216.0%)	p < 0.001 (***)
Daily Energy Consumption (kWh/day)	2.88 kWh	1.64 kWh	-1.24 kWh (-43.06%)	p < 0.001 (***)

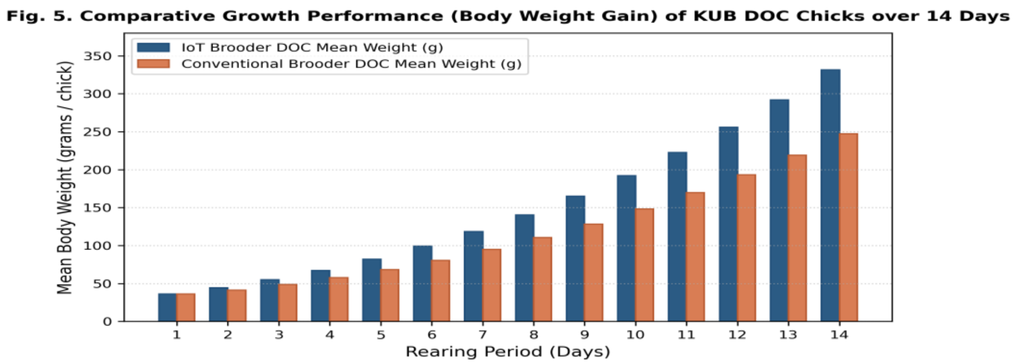

Fig. 5. Daily mean body weight progression of KUB DOC chicks over the 14-day experimental brooding period.

The statistical findings in Table 3 and Fig. 5 conclusively validate the transformative zootechnical impact of the IoT-driven closed-loop brooder. While initial body weights on Day 1 were virtually identical (36.10 g vs. 36.20 g; $p = 0.852$), the growth trajectories diverged substantially from Day 4 onwards as physiological metabolic demands accelerated. By Day 14, chicks reared under the IoT microclimate achieved a mean body weight of 331.50 ± 12.40 g, representing a highly significant 34.10% increase over the conventional group (247.20 ± 15.80 g; $p < 0.001$).

From a nutritional physiology standpoint, the Feed Conversion Ratio (FCR)—defined as total feed intake divided by body weight gain—improved from 1.62 in the conventional brooder to an outstanding 1.24 in the IoT brooder (a 23.46% efficiency gain). In the conventional brooder, sub-optimal nocturnal temperatures forced the chicks to partition dietary metabolisable energy toward endogenous thermogenesis and basal metabolic heat generation rather than somatic skeletal-muscular protein accretion. By maintaining precise homeostatic thermal equilibrium (TSI = 98.6%), the IoT system maximized net energy retention for somatic growth.

Crucially, cumulative neonatal mortality dropped from 8.00% in the control group to just 1.00% in the IoT brooder (an 87.5% reduction in flock mortality). Necropsy examinations of dead chicks from the control group revealed severe pulmonary congestion and unabsorbed vitelline sacs resulting from chronic hypothermic exposure. Furthermore, the closed-loop intermittent heating control reduced daily electrical energy consumption by 43.06% (1.64 kWh/day vs. 2.88 kWh/day in the continuously powered incandescent system), demonstrating compelling operational cost efficiency and environmental sustainability.

IV. CONCLUSION

This research has successfully engineered, implemented, and empirically validated an intelligent, cyber-physical IoT microclimate monitoring and closed-loop control system for KUB Day-Old Chick (DOC) brooding facilities. By coupling an industrial-grade Aosong DHT20 I2C sensor with an explicit 12V DC power rail voltage monitoring subsystem and an ESP32 edge microcontroller, the system overcomes the critical timing vulnerabilities, signal drift, and electrical instability inherent in legacy agricultural IoT architectures. Static metrological calibration confirmed high sensor precision, achieving a temperature MAE of 0.194 °C ($R^2 = 0.9998$) and voltage precision of 0.021 V ($R^2 = 0.9999$). Dynamic 24-hour field trials under severe tropical ambient swings demonstrated superior microclimatic regulation, sustaining internal brooder temperatures at 33.52 ± 0.38 °C (TSI = 98.6%) and relative humidity at 65.4 ± 2.8% while rejecting nocturnal cold shocks and diurnal heat spikes. Over a 14-day live biological trial with n = 200 KUB DOC chicks, the automated system reduced cumulative neonatal mortality from 8.0% to 1.0%, enhanced final chick body weight by 34.1% (331.5 g vs. 247.2 g), optimized the Feed Conversion Ratio to 1.24 (vs. 1.62), and decreased electrical energy consumption by 43.1%. Future work will focus on integrating edge-based TinyML computer vision for automated chick behavioral clustering classification and integrating photovoltaic-battery hybrid microgrids for off-grid rural farming independence.

V. ACKNOWLEDGMENTS

The authors express their sincere gratitude to the Mechanical Engineering Universitas Persatuan Guru Republik Indonesia Semarang for providing institutional research facilities, funding support, and laboratory equipment. Special appreciation is extended to the Mechatronics and Robotics Research Group and local poultry breeding partners for their technical collaboration during the field experimental trials.

REFERENCES

[1] S. Neethirajan, "Recent advances in wearable sensors and internet of things for precision livestock farming," Computers and Electronics in Agriculture, vol. 177, p. 105689, 2020. https://doi.org/10.1016/j.compag.2020.105689

[2] D. Berckmans, "General introduction to precision livestock farming," Animal Frontiers, vol. 7, no. 1, pp. 6–11, 2017. https://doi.org/10.2527/af.2017.0102

[3] T. Norton, C. Chen, M. L. V. Larsen, and D. Berckmans, "Precision livestock farming: Building 'smart-farms' that design with not just by technology," Animal Frontiers, vol. 9, no. 2, pp. 12–19, 2019. https://doi.org/10.1093/af/vfz005

[4] T. B. Iskandar, J. Sartika, and E. J. Sembiring, "Performance and genetic characteristics of KUB chicken (Kampung Unggul Balitbangtan) under tropical smallholder conditions," Indonesian Journal of Animal and Veterinary Sciences, vol. 26, no. 3, pp. 112–122, 2021.

[5] H. A. Olanrewaju, J. L. Purswell, S. D. Collier, and S. L. Branton, "Interactive effects of ambient temperature and relative humidity on physiological responses and growth performance in broilers," International Journal of Poultry Science, vol. 14, no. 5, pp. 240–248, 2015.

[6] I. F. M. Amaral, B. B. L. Medeiros, F. A. Damasceno, and J. A. O. Saraz, "Brooding phase environmental management and thermal comfort indices in poultry production: A comprehensive review," Environmental Science and Pollution Research, vol. 28, no. 12, pp. 14321–14335, 2021.

[7] A. Prawoto, D. Ratnaningsih, M. F. Setiyawan, M. R. Gunarti, and S. D. Robbi, "Design and Construction of an Arduino-Based Main Engine Overheating Detection Prototype," International Journal of Science and Environment (IJSE), vol. 6, no. 1, pp. 1171–1182, 2026.

[8] Pujianto, M. Z. Z. Muhtadi, and M. O. Lambiombir, "Design of an MPPT Monitoring System for a Solar Power Plant Based on the Internet of Things Using ESP32 and ThingSpeak," International Journal of Science and Environment (IJSE), vol. 6, no. 1, pp. 1870–1878, 2026.

[9] A. Soleha, J. Lianda, and Adam, "IoT-Based Solar Power Plant Parameter Monitoring System," International Journal of Science and Environment (IJSE), vol. 6, no. 1, pp. 1418–1424, 2026.

[10] D. Hercog, T. Lerher, M. Truntič, and O. Težak, "Design and implementation of ESP32-based IoT devices," Sensors, vol. 23, no. 15, p. 6739, 2023. https://doi.org/10.3390/s23156739

[11] M. A. A. Al-qaness, A. A. Abbasi, H. Zheng, and M. A. Elaziz, "An efficient IoT-based smart poultry monitoring and management system using edge computing," IEEE Internet of Things Journal, vol. 9, no. 21, pp. 21875–21886, 2022. https://doi.org/10.1109/JIOT.2022.3182104

[12] J. S. Tutuko, A. Prawoto, D. Ratnaningsih, A. E. Kristiyono, and S. D. Robbi, "Air Compressor Design and Construction With ESP32 Based Microcontroller Monitoring System," International Journal of Science and Environment (IJSE), vol. 6, no. 1, pp. 1134–1140, 2026.

[13] R. G. Mahale, N. P. Mahale, and P. K. Sonar, "Design and development of IoT based poultry farm monitoring and automated climate control system," Computers and Electronics in Agriculture, vol. 188, p. 106342, 2021. https://doi.org/10.1016/j.compag.2021.106342

[14] N. J. Beltrán Castañón, F. Chura Acero, J. Ramos Cutipa, and E. Cruz Ticona, "A Low-Cost Wireless Monitoring System for Photovoltaic Systems: Performance Analysis and Potential Application," Energies, vol. 18, no. 9, p. 2279, 2025.

[15] C. F. Bustamante, J. A. O. Saraz, and K. S. O. Rocha, "CFD simulation of thermal distribution and air velocity inside a smart broiler brooding house under variable ventilation," Biosystems Engineering, vol. 210, pp. 245–258, 2021. https://doi.org/10.1016/j.biosystemseng.2021.08.014

[16] W. Khalid, M. Jamil, A. A. Khan, and Q. Awais, "Open-source internet of things-based supervisory control and data acquisition system for photovoltaic monitoring and control using HTTP and TCP/IP protocols," Energies, vol. 17, no. 16, p. 4083, 2024.

[17] Y. Saleem, N. Crespi, M. H. Rehmani, and R. Copeland, "Internet of Things-aided smart grid: Technologies, architectures, applications, prototypes, and future research directions," Future Generation Computer Systems, vol. 101, pp. 218–236, 2019. https://doi.org/10.1016/j.future.2019.06.017

[18] M. R. Al-Mashhadani, S. S. Hameed, and K. A. Jasim, "Experimental investigation of energy-efficient smart brooding system with automated temperature control for poultry farming," Energy and Buildings, vol. 254, p. 111580, 2022. https://doi.org/10.1016/j.enbuild.2021.111580

[19] V. R. Sastri, "Applications of advanced sensor arrays in environmental bio-monitoring," Modern Aspects of Sensor Science, vol. 4, pp. 893–981, 2023.

[20] E. F. Orumwense and K. Abo-Al-Ez, "Internet of Things for smart energy systems: A review on its applications, challenges and future trends," AIMS Electronics and Electrical Engineering, vol. 7, no. 1, pp. 50–74, 2023. https://doi.org/10.3934/electreng.2023004.